Curvature instability of a vortex ring (Mathematical Analysis in Fluid and Gas Dynamics)

AUTHOR(S):

Fukumoto, Yasuhide; Hattori, Yuji

CITATION:

Fukumoto, Yasuhide ...[et al]. Curvature instability of a vortex ring (Mathematical Analysis in Fluid and Gas Dynamics). 数理解析研究所講究録 2004, 1353: 143-162

ISSUE DATE:

2004-01

URL:

http://hdl.handle.net/2433/25152

数理解析研究所講究録 1353 巻 2004 年 143-162

Curvature instability of a vortex ring

九大数理　福本 康秀 (Yasuhide Fukumoto)
Graduate School of Mathematics, Kyushu Univ.
九工大工　服部 裕司 (Yuji Hattori)
Faculty of Engineering, Kyushu Institute of Technology

1 Introduction

Vortex rings are invariably susceptible to wavy distortions, leading sometimes to violent wiggles and eventually to disruption. It prevails that the *Moore-Saffman-Tsai-Widnall instability*, being abbreviated as the MSTW instability, is responsible for genesis of unstable waves (Widnall, Bliss & Tsai 1974; Moore & Saffman 1975; Tsai & Widnall 1976; Widnall & Tsai 1977). Remember that this is an instability for a straight vortex tube subjected to a straining field.

When viewed locally, a thin vortex ring looks like a straight tube. For simplicity, we restrict our attention to the *Rankine vortex*, a circular core of uniform vorticity. Because of circular-cylindrical symmetry, the Rankine vortex is neutrally stable and supports a family of three-dimensional waves of infinitesimal amplitude, being well known as the *Kelvin waves*. The vortex ring induces, on itself, not only a local uniform flow that drives a translational motion as a whole, but also a local straining field akin to a pure shear, in the meridional plane, with principal axes tilted by $\pi/4$ from the symmetric axis (Widnall, Bliss & Tsai 1974). This is a quadrupole field proportional to $\cos 2\theta$ and $\sin 2\theta$, in terms of local polar coordinates (r, θ) in the meridional plane, with its origin at the core center and with $\theta = 0$ along the traveling direction. This field breaks the circular symmetry of the core by deforming it into ellipse, and feeds parametric resonance between two Kelvin waves whose azimuthal wavenumbers are separated by 2 (Moore & Saffman 1975, Tsai & Widnall 1976; Eloy & Le Dizès 2001; Fukumoto 2003). In the short-wavelength regime, the MSTW instability crosses over to the *elliptical instability* found by Bayly (1986) and Waleffe (1990).

However this might be a picture too crude to fit into a curved vortex tube. The asymptotic solution of the Navier-Stokes or the Euler equations for a thin vortex ring in powers of a small parameter ϵ, the ratio of the core to the ring radii, starts with a circular-cylindrical vortex tube at $O(\epsilon^0)$. A vortex ring is featured by curvature of vortex lines. This feature manifests itself, at $O(\epsilon^1)$, as a local *dipole field* proportional to $\cos\theta$ and $\sin\theta$. The quadrupole field comes merely as a correction at $O(\epsilon^2)$ (Fukumoto & Moffatt 2000; Fukumoto 2002). Despite its dominance, the dipole field has not attracted as much attention as it deserves. This investigation addresses a possible instability when the dipole field comes into play.

According to Krein's theory of parametric resonance in Hamiltonian systems (MacKay 1986), a single Kelvin wave cannot be fed by perturbations breaking the circular symmetry. An instability becomes permissible only for superposition of at least two modes with the same wavenumber and the same frequency. Subjected to the dipole field, two Kelvin waves with angular dependence $e^{im\theta}$ and $e^{in\theta}$ can cooperatively be amplified at the intersection points of dispersion curves if the condition $|m-n|=1$ is met.

A formulation of the linear stability analysis was fully performed by Widnall & Tsai (1977), hereinafter being referred to as WT77, but the dipole effect has gone untouched. Fukumoto & Hattori (2002) verified that a combination of the *axisymmetric* ($m=0$) and the *bending* ($n=1$) waves indeed leads to parametric resonance. The local stability analysis of Hattori & Fukumoto (2003) disclosed the existence of more unstable resonance via the dipole field.

These results stimulate us to exhaust all possible resonant azimuthal-wavenumber pairs $(m, m+1)$ of Kelvin waves. It will be shown that the most dangerous instability mode takes place in the limit of $m \to \infty$. Contrary to the instability of quadrupole-field origin, all of multiple eigenvalues do not result in resonance. The necessary condition for instability, brought out by Krein's theory, is either that the eigenvalue collision occurs between a positive- and a negative-energy modes or that the collision eigenvalue is zero. Energy of the Kelvin waves, which was calculated by Fukumoto (2003), is instrumental in making distinction between resonant and non-resonant eigenvalue collisions.

In §2, we give a concise description of the problem setting for linear stability analysis. The Kelvin waves are recalled in Appendix A. Section 3 seeks the solution of the linearized Euler equations. Remarkably Kelvin's vortex ring admits a closed-form solution, in terms only of the Bessel and the modified Bessel functions, for the disturbance velocity field, and so is for the growth rate and the width of unstable wavenumber band. The detailed form of solution is relegated to Appendix B. In §4, we present a numerical example and the short-wave asymptotics is dealt with in §5.

The detail is described in Fukumoto & Hattori (2004).

2 Setting of linear stability problem

The formulation of the global linear stability analysis in three dimensions was made by WT77. We employ its notation.

Kelvin's vortex ring is a thin axisymmetric vortex ring, in an incompressible inviscid fluid, with vorticity proportional to the distance from the axis of symmetry. We assume that the ratio ϵ of core rsdius σ to ring radius R is very small:

$$\epsilon = \sigma/R \ll 1 . \tag{2.1}$$

Introduce toroidal coordinates (r, θ, s) comoving with the ring. In the meridional plane $s=0$, the origin $r=0$ is maintained at the center of the circular core and the angle θ is measured from the direction parallel to the axis of symmetry, the x-axis say. The center

circle penetrating inside the toroidal ring is parameterized by the arclength s. The global Cartesian coordinates (x, y, z) are then expressed by

$$x = r\cos\theta\,, \quad y = (R + r\sin\theta)\cos s\,, \quad z = (R + r\sin\theta)\sin s\,. \tag{2.2}$$

We normalise the radial coordinate r by the core radius σ, the velocity by the maximum azimuthal velocity $\Gamma/2\pi\sigma$ with Γ being the circulation, the time t by $2\pi\sigma^2/\Gamma$ and the pressure by $\rho_f(\Gamma/2\pi\sigma)^2$ with ρ_f being the density of fluid. Let the r and θ components of velocity field be U and V, respectively, and the pressure be P inside the core ($r < 1$). The velocity potential for the exterior irrotational flow is denoted by Φ.

The basic flow is expanded in powers of ϵ, the first-order truncation of which takes the form:

$$\begin{aligned} U &= \epsilon U_1(r,\theta) + \cdots\,, \quad V = V_0(r) + \epsilon V_1(r,\theta) + \cdots\,, \\ P &= P_0(r) + \epsilon P_1(r,\theta) + \cdots \quad \text{for } r < 1\,, \qquad (2.3) \\ \Phi &= \Phi_0(\theta) + \epsilon\Phi_1(r,\theta) + \cdots \quad \text{for } r > 1\,. \qquad (2.4) \end{aligned}$$

The leading-order flow is the Rankine vortex as expressed, in dimensionless form, by

$$V_0 = r\,, \quad P_0 = \frac{1}{2}(r^2 - 1)\,, \quad \Phi_0 = \theta\,. \tag{2.5}$$

The first-order flow field is a dipole field:

$$\begin{aligned} U_1 &= \frac{5}{8}(1 - r^2)\cos\theta\,, \quad V_1 = \left(-\frac{5}{8} + \frac{7}{8}r^2\right)\sin\theta\,, \quad P_1 = \left(-\frac{5}{8}r + \frac{3}{8}r^3\right)\sin\theta\,, \\ \Phi_1 &= \left(\frac{1}{8}r - \frac{3}{8r} - \frac{1}{2}r\log r\right)\cos\theta\,. \end{aligned} \tag{2.6}$$

To this order, circular form of core boundary ($r = 1$) remains intact.

We inquire into evolution of three-dimensional disturbances of infinitesimal amplitude superposed on the above steady flow. Following the prescription of Moore & Saffman (1975) and Tsai & Widnall (1976), we expand the disturbance velocity $\tilde{v}$, the disturbance pressure $\tilde{p}$ and the external disturbance velocity-potential $\tilde{\phi}$ in powers of ϵ to first order

$$\begin{aligned} \tilde{v} &= \mathrm{Re}[(v_0 + \epsilon v_1 + \cdots)e^{i(ks-\omega t)}]\,, \quad \tilde{p} = \mathrm{Re}[(\pi_0 + \epsilon\pi_1 + \cdots)e^{i(ks-\omega t)}]\,, \\ \tilde{\phi} &= \mathrm{Re}[(\phi_0 + \epsilon\phi_1 + \cdots)e^{i(ks-\omega t)}]\,, \end{aligned} \tag{2.7}$$

where the symbol Re designates the real part. In keeping with this form, the wavenumber k and the frequency ω, nondimensionalised by $1/\sigma$ and $\Gamma/(2\pi\sigma^2)$ respectively, are also expanded as

$$k = k_0 + \epsilon k_1 + \cdots\,, \quad \omega = \omega_0 + \epsilon\omega_1 + \cdots\,. \tag{2.8}$$

The disturbed edge of the core is expanded as

$$r = 1 + \tilde{f}_0(\theta, s, t) + \epsilon\tilde{f}_1(\theta, s, t) + \cdots\,. \tag{2.9}$$

3 Effect of dipole field

The flow field $\boldsymbol{v}_0$, π_0 and ϕ_0 and the dispersion relation $\omega_0 = \omega_0(k_0)$ of Kelvin waves are accommodated in Appendix A (see, for example, Saffman 1992; Fukumoto 2003). Our concern lies in the modification of Kelvin's dispersion relation due to symmetry-breaking action of the $O(\epsilon)$ dipole field.

3.1 Governing equations

We denote the toroidal component of disturbance velocity by w. The amplitude vector $\boldsymbol{v}_1$ of disturbance velocity and the amplitude π_1 of disturbance pressure of $O(\epsilon)$ are governed, inside the core ($r < 1$), by

$$-i\omega_0 u_1 + \frac{\partial u_1}{\partial r} - 2v_1 + \frac{\partial \pi_1}{\partial r} = \left(i\omega_1 - \frac{\partial U_1}{\partial r}\right) u_0 - U_1 \frac{\partial u_0}{\partial r} - \frac{V_1}{r}\frac{\partial u_0}{\partial \theta} - \left(\frac{1}{r}\frac{\partial U_1}{\partial \theta} - \frac{2V_1}{r}\right) v_0 , \tag{3.1}$$

$$-i\omega_0 v_1 + 2u_1 + \frac{\partial v_1}{\partial \theta} + \frac{1}{r}\frac{\partial \pi_1}{\partial \theta} = \left(i\omega_1 - \frac{1}{r}\frac{\partial V_1}{\partial \theta} - \frac{U_1}{r}\right) v_0 - \left(\frac{\partial V_1}{\partial r} + \frac{V_1}{r}\right) u_0 - U_1 \frac{\partial v_0}{\partial r} - \frac{V_1}{r}\frac{\partial v_0}{\partial \theta} , \tag{3.2}$$

$$-i\omega_0 w_1 + \frac{\partial w_1}{\partial \theta} + ik_0 \pi_1 = -ik_1 \pi_0 + (i\omega_1 - r\cos\theta) w_0 - \frac{V_1}{r}\frac{\partial w_0}{\partial \theta} - U_1 \frac{\partial w_0}{\partial r} + ik_0 r \sin\theta \pi_0 , \tag{3.3}$$

$$\frac{\partial u_1}{\partial r} + \frac{u_1}{r} + \frac{1}{r}\frac{\partial v_1}{\partial \theta} + ik_0 w_1 = -\sin\theta u_0 - \cos\theta v_0 + ik_0 r \sin\theta w_0 . \tag{3.4}$$

The last one is the equation of continuity. The amplitude function ϕ_1 of velocity potential for the disturbance flow of $O(\epsilon)$, outside the core ($r > 1$), satisfies

$$\frac{\partial^2 \phi_1}{\partial r^2} + \frac{1}{r}\frac{\partial \phi_1}{\partial r} + \frac{1}{r^2}\frac{\partial^2 \phi_1}{\partial r^2} - k_0^2 \phi_1 = 2k_0 k_1 \phi_0 - \sin\theta \frac{\partial \phi_0}{\partial r} - \frac{\cos\theta}{r}\frac{\partial \phi_0}{\partial \theta} - 2k_0^2 r \sin\theta \phi_0 . \tag{3.5}$$

The boundary conditions require that the normal component of velocity and the pressure be continuous across the interface ($r = 1$) of the core:

$$\begin{aligned} u_1 &= \frac{\partial \phi_1}{\partial r} , \\ \pi_1 - i\omega_0 \phi_1 + \frac{\partial \phi_1}{\partial \theta} &= i\omega_1 \phi_0 - \frac{\partial \Phi_1}{\partial \theta}\frac{\partial \phi_0}{\partial \theta} . \end{aligned} \tag{3.6}$$

The shape of disturbed core boundary is found from

$$i\omega_0 f_1 - \frac{\partial f_1}{\partial \theta} + u_1 = -i\omega_1 f_0 + V_1 \frac{\partial f_0}{\partial \theta} - \frac{\partial U_1}{\partial r} f_0 . \tag{3.7}$$

The right-hand sides of (3.1)–(3.7) include the coupling of Kelvin waves with the dipole field (2.6) of $O(\epsilon)$. We delineate WT77's formulation, as generalised to higher azimuthal-wavenumber resonance.

Suppose that a pair of Kelvin waves whose azimuthal wavenumbers differ by 1 are simultaneously sent to $O(\epsilon^0)$:

$$\boldsymbol{v}_0 = \boldsymbol{v}_0^{(1)} e^{im\theta} + \boldsymbol{v}_0^{(2)} e^{i(m+1)\theta} . \tag{3.8}$$

Here and hereafter, we make use of superscripts of (1) and (2) for the m and the $m+1$ waves respectively. In view of the dipole field on the right-hand sides of (3.1)–(3.5) and the boundary conditions (3.6), the wave excited at $O(\epsilon)$ is found to possess the following angular dependence:

$$\boldsymbol{v}_1 = \boldsymbol{v}_1^{(1)} e^{im\theta} + \boldsymbol{v}_1^{(2)} e^{i(m+1)\theta} + \boldsymbol{v}_1^{(3)} e^{i(m-1)\theta} + \boldsymbol{v}_1^{(4)} e^{i(m+2)\theta} . \tag{3.9}$$

The similar form is posed on π_0, ϕ_0 and π_1, ϕ_1. Excitation, at $O(\epsilon)$, of a pair of waves with the same azimuthal wavenumbers as at $O(\epsilon^0)$ implies a possibility of parametric resonance.

The leading-order disturbance is, from Appendix A,

$$\begin{aligned} \phi_0 &= K_m(k_0 r)\alpha_0^{(1)} e^{im\theta} + K_{m+1}(k_0 r)\alpha_0^{(2)} e^{i(m+1)\theta} , \\ \pi_0 &= J_m(\eta_1 r)\beta_0^{(1)} e^{im\theta} + J_{m+1}(\eta_2 r)\beta_0^{(2)} e^{i(m+1)\theta} , \end{aligned} \tag{3.10}$$

where J_m and K_m are, respectively, the Bessel function of the first kind and the modified Bessel function of the second kind, m being their order, $\alpha_0^{(1)}$, $\alpha_0^{(2)}$, $\beta_0^{(1)}$ and $\beta_0^{(2)}$ are constants, and η_1 and η_2 are the radial wavenumbers of the m and the $m+1$ waves respectively as defined by (A.4) and (A.5). Likewise, the interior velocity field (u_0, v_0, w_0) is expressible as superposition of the expressions (A.3) for the m and $m+1$ waves.

Upon substituting from (3.10), (3.5) is integrated to yield

$$\begin{aligned} \phi_1^{(1)} &= K_m(k_0 r)\alpha_1^{(1)} - k_1 r K_{m+1}(k_0 r)\alpha_0^{(1)} \\ &\quad + \frac{i}{4}\left\{k_0 r^2 K_m(k_0 r) + (2m+1) r K_{m+1}(k_0 r)\right\}\alpha_0^{(2)} , \end{aligned} \tag{3.11}$$

$$\begin{aligned} \phi_1^{(2)} &= K_{m+1}(k_0 r)\alpha_1^{(2)} - k_1 r K_m(k_0 r)\alpha_0^{(2)} \\ &\quad + \frac{i}{4}\left\{(2m+1) r K_m(k_0 r) - k_0 r^2 K_{m+1}(k_0 r)\right\}\alpha_0^{(1)} , \end{aligned} \tag{3.12}$$

where $\alpha_1^{(1)}$ and $\alpha_1^{(2)}$ are constants imparted to the homogeneous parts of solution.

Analytical handling of the interior field becomes feasible by collapsing (3.1)–(3.4), at the outset, to second-order ordinary differential equations for the disturbance pressure $\pi_1^{(1)}$ are $\pi_1^{(2)}$. After some computer algebra, we are left with

$$\begin{aligned} L^{(1)}[\pi_1^{(1)}] = \left\{\frac{8k_0^2\omega_1}{(\omega_0 - m)^3} - \frac{2k_1}{k_0}\eta_1^2\right\} J_m(\eta_1 r)\beta_0^{(1)} - i\Bigg\{\Bigg[\frac{1}{2} + \frac{3m}{2(\omega_0 - m - 1)} \\ - \frac{5k_0^2}{4}\Big(\frac{1}{(\omega_0 - m)^2} - \frac{1}{(\omega_0 - m - 1)^2}\Big)(r^2 - 1)\Bigg]\eta_2 J_m(\eta_2 r) \\ + \Bigg[1 + \frac{8\omega_0 - 9m - 1}{2(\omega_0 - m)^2} - \frac{7\omega_0 - 9m - 19}{4(\omega_0 - m - 1)^2}\Bigg] k_0^2 r J_{m+1}(\eta_2 r)\Bigg\}\beta_0^{(2)} , \end{aligned} \tag{3.13}$$

$$L^{(2)}[\pi_1^{(2)}] = \left\{\frac{8k_0^2\omega_1}{(\omega_0-m-1)^3} - \frac{2k_1}{k_0}\eta_2^2\right\}J_{m+1}(\eta_2 r)\beta_0^{(2)} + \frac{i}{4}\left\{\left[4 + \frac{7\omega_0-9m+10}{(\omega_0-m)^2}\right.\right.$$
$$\left.-\frac{2(8\omega_0-9m-8)}{(\omega_0-m-1)^2}\right]k_0^2 r J_m(\eta_2 r) - \left[2 + \frac{6(m+1)}{\omega_0-m-2}\right.$$
$$\left.\left.+5k_0^2\left(\frac{1}{(\omega_0-m)^2} - \frac{1}{(\omega_0-m-1)^2}\right)(r^2-1)\right]\eta_1 J_{m+1}(\eta_1 r)\right\}\beta_0^{(1)}, \tag{3.14}$$

where

$$L^{(i)} = \frac{d^2}{dr^2} + \frac{1}{r}\frac{d}{dr} - \frac{m_i^2}{r^2} + \eta_i^2 \quad (i=1,2). \tag{3.15}$$

The boundary conditions (3.6) read, for the m wave,

$$u_1^{(1)} - \frac{\partial\phi_1^{(1)}}{\partial r} = 0, \quad \pi_1^{(1)} - i(\omega_0-m)\phi_1^{(1)} = i\omega_1\phi_0^{(1)} + \frac{m+1}{8}\phi_0^{(2)}, \tag{3.16}$$

and, for the $m+1$ wave,

$$u_1^{(2)} - \frac{\partial\phi_1^{(2)}}{\partial r} = 0, \quad \pi_1^{(2)} - i(\omega_0-m-1)\phi_1^{(2)} = i\omega_1\phi_0^{(2)} - \frac{m}{8}\phi_0^{(1)}. \tag{3.17}$$

3.2 Disturbance field and growth rate

WT77 skipped the solution for $\boldsymbol{v}_1$. We are now ready to build the solution of (3.13) and (3.14) and to calculate the $O(\epsilon)$ correction ω_1 to the eigenfrequency from the boundary conditions (3.16) and (3.17).

By appealing to symbolic calculus, Mathematica say, the solution of (3.13) and (3.14) is obtained in closed form solely in terms of the Bessel functions. The resulting expressions for $\pi_1^{(1)}$, $\pi_1^{(2)}$, $u_1^{(1)}$ and $u_1^{(2)}$, the enforcement of the boundary conditions (3.16) and (3.17) and the solvability conditions on them are written down in Appendix B.

We recapitulate the procedure of Moore & Saffman (1975) and Tsai & Widnall (1976). Simultaneous excitation of at least two Kelvin waves is requisite for instability, being indicative of parametric resonance. The postulation that the solvability conditions (B.7) and (B.8) have a nontrivial solution of $\beta_0^{(1)} \neq 0$ and $\beta_0^{(2)} \neq 0$ gives rise to ω_1. Instability is implied when $\mathrm{Im}[\omega_1] > 0$ and we write its growth rate as $\sigma_1 = |\mathrm{Im}[\omega_1]|$. In case of instability, the growth rate takes its local maximum value $\sigma_{1\max}$ at $k = k_0$, namely $k_1 = 0$, and $\mathrm{Im}[\omega_1] > 0$ only over a limited wavenumber range of width $2\epsilon\Delta k_1$ centered on $k = k_0$. The desired formulae of $\sigma_{1\max}$ and Δk_1 are gained from (B.7) and (B.8) as

$$\sigma_{1\max}^2 = -\frac{(\omega_0-m)^3(\omega_0-m-1)^3(\omega_0-m+1)(\omega_0-m+2)(\omega_0-m-2)(\omega_0-m-3)}{1024k_0^4(2\omega_0-2m-1)^4}$$
$$\times\frac{h^2}{f^{(1)}f^{(2)}}, \tag{3.18}$$

$$\Delta k_1^2 = -\frac{(\omega_0-m)^3(\omega_0-m-1)^3(\omega_0-m+1)(\omega_0-m+2)(\omega_0-m-2)(\omega_0-m-3)}{1024k_0^2(2\omega_0-2m-1)^4}$$
$$\times\frac{f^{(1)}f^{(2)}h^2}{d^2}, \tag{3.19}$$

where

$$d = (\omega_0 - m)(\omega_0 - m + 2)(\omega_0 - m - 2) f^{(2)} g^{(1)} - (\omega_0 - m - 1)(\omega_0 - m + 1)(\omega_0 - m - 3) f^{(1)} g^{(2)}, \tag{3.20}$$

and the form of $f^{(1)}$, $f^{(2)}$, $g^{(1)}$, $g^{(2)}$ and h is provided by (B.9)–(B.13).

4 Example

4.1 Resonance between the $0, 1$ waves

To give an illustration, we carry through numerical computation of stability characteristics for the copling between the axisymmetric ($m = 0$) and the bending ($m = 1$) waves. The dispersion relation of Kelvin waves of $m = 0$ (dashed lines) and $m = 1$ (solid lines) is displayed in figure 1. The isolated branch of $m = 1$, starting from $\omega_0 = 0$, is drawn with a thick solid line. Infinitely many branches emanate from $(k_0, \omega_0) = (0, 1)$ for $m = 1$ among which twenty branches, ten upgoing and ten downgoing, are drawn. Theses modes are named the *radial modes* since the eigenfunctions have nontrivial radial nodal structure. A wave with $|\omega_0| > 1$ rotates faster than the basic circulatory flow and is called a *cograde* mode, which is distinguished from a wave with $|\omega_0| < 1$, a *retrograde* mode (Saffman 1992). In contrast, an isolated branch and the counterpart of retrograde modes are missing for the axisymmetric mode. Given the wavenumber k_0, the modes with ω_0 and with $-\omega_0$ share a common property of cograde radial mode.

A positive axisymmetric mode ($\omega_0 > 0$) crosses every retrograde mode of $m = 1$ once, and may cross, twice, some of higher cograde branches of $m = 1$. A negative axisymmetric mode ($\omega_0 < 0$) collides, if its branch index is high enough, with some of retrograde radial modes of $m = 1$, twice per each. The isolated mode of $m = 1$ crosses branches of $m = 0$ at small values of k_0.

The growth rate (3.18) is calculated at many of intersection points. Collision of eigenvalues of the $0, 1$ waves does not necessarily result in instability. Stability is lost only at intersection points between positive branches of $m = 0$ and retrograde radial modes of $m = 1$, and otherwise this is not the case. This behaviour lies in stark contrast with that of the MSTW instability. In the latter case, every eigenvalue collision invites parametric resonance (Eloy & Le Diès 2001; Fukumoto 2003). The energetics holds the key to distinguish non-resonant collisions from resonant ones, as will be described in §4.3.

In Table 1, we list the evaluated values of the growth rate and the unstable band-width for low wavenumbers. The first three rows correspond to the first three intersection points of the first positive axisymmetric mode ($m = 0$) with retrograde radial modes of $m = 1$, and are marked with circles in figure 1. The next three rows are along the second mode of $m = 0$ (thick dotes), and the last three along the third mode of $m = 0$ (squares). Since the torus center is a circle of radius R, an unstable mode is realizable only when the arclength $2\pi R$ coincides with some integral multiple of a half of the wavelength $2\pi/k_0$. The unstable band-width needs to be sufficiently broad.

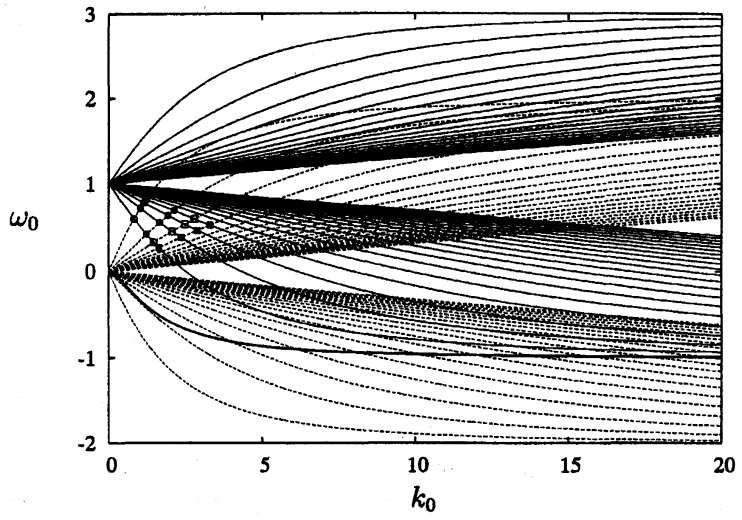

Figure 1: Dispersion relation of the axisymmetric wave $m = 0$ (dashed lines) and the helical wave $m = 1$ (solid lines) on the Rankine vortex. The isolated branch of $m = 1$ is shown with a thick line.

k_0	ω_0	$\sigma_{1\max}$	Δk_1
0.8134868347	0.5970895378	0.05434123370	0.1022075453
1.018687659	0.7162537484	0.007063858086	0.01725321243
1.136862167	0.7794574187	0.008676095366	0.02449637577
1.224505620	0.4217998862	0.03931853915	0.1093080415
1.650449151	0.5528357882	0.03769686682	0.1381880078
1.927505750	0.6329096309	0.004366456551	0.01889368333
1.464572874	0.3290672352	0.02466638188	0.08406115354
2.059092345	0.4537065585	0.01547299060	0.07032354299
2.472533079	0.5364030938	0.03273541819	0.1773468081

Table 1: The maximum growth rate $\epsilon\sigma_{1\max}$ and the half-width $\epsilon\Delta k_1$ of unstable wavenumber band to $O(\epsilon)$ for (0,1) resonance

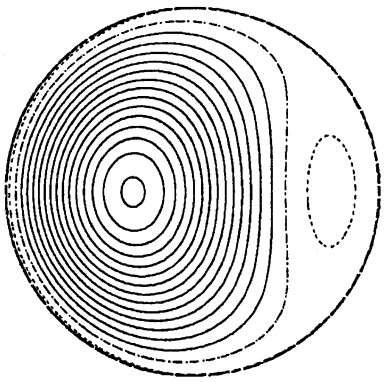

Figure 2: Contour of disturbance toroidal velocity field w_0 on the meridional plane $k_0 s = \omega_0 t$ for the first principal mode of the $(0,1)$ resonance. The dashed line depicts the core boundary $r = 1$.

Large growth rate is maintained to short wavelengths at intersection points between the i-th branch of $m = 0$ and the i-th branch of the retrograde radial modes of $m = 1$. This sequence belongs to what we call the *principal modes*. The origin $(k_0, \omega_0) = (0, 0)$ is the intersection point between the isolated branch of $m = 1$ and all branches of $m = 0$. This is considered to be a neutrally stable point (Fukumoto & Hattori 2004).

Among the intersection points examined so far, the maximum of growth rate is attained at the first principal mode, namely at $(k_0, \omega_0) \approx (0.8134868347, 0.5970895378)$, though the maximum value $\sigma_{1\max} \approx 0.05434123370$ is not very large. The corresponding flow field is calculated, to $O(\epsilon^0)$, from (3.8) with $\boldsymbol{v}_0^{(1)}$ and $\boldsymbol{v}_0^{(2)}$ provided in Appendix A. The solvability conditions bring in $\beta_0^{(2)}/\beta_0^{(1)} \approx 0.7276318666$ at this point.

The contour of toroidal velocity w_0 on the crosssectional plane $k_0 s = \omega_0 t$ is drawn in figure 2. Only the interior region $(r < 1)$ is shown. A strong toroidal or axial current is induced over a massive region with the location of peak velocity deviated backward from the core center, and is accompanied by a minor counter current in the front part of the core. The location of peak velocity winds helically around the torus center, and executes a circulatory motion around the center. Figure 3(a) displays the disturbance vorticity field $(\omega_{0r}, \omega_{0\theta})$ of $O(\epsilon^0)$ projected to the same crosssectional plane. The contour of toroidal vorticity ω_{0s} is shown in figure 3(b). The ring-like vorticity structure in figure 3(a) corresponds to strong toroidal flow in figure 2. The toroidal vorticity is large at points where the toroidal current is week.

We reason that, as with the cases of the elliptical instability (Waleffe 1990) and of the instability due to multi-polar strain (Eloy & Le Dizès 2001), the instability mechanism is attributable to parallelization between the stretching direction of local shear and the disturbance vorticity. Fukumoto & Hattori (2002) calculated the probability distribution

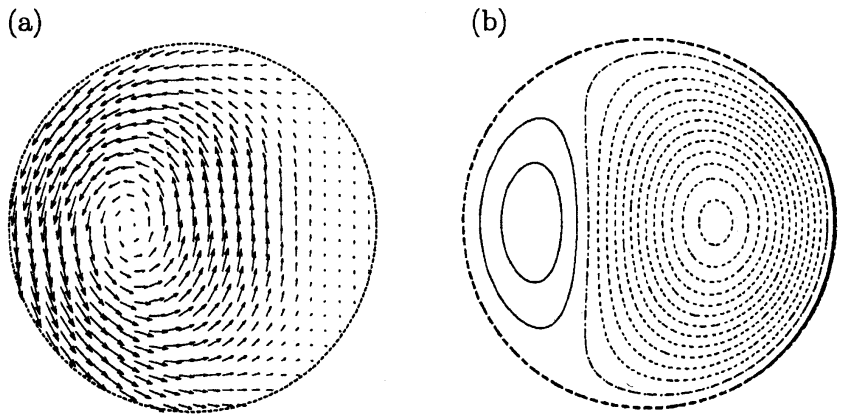

Figure 3: Disturbance vorticity field in the meridional plane $k_0 s = \omega_0 t$ of the first principal mode of the $(0,1)$ resonance. (a) The meridional components $(\omega_{0r}, \omega_{0\theta})$. (b) Contour of disturbance toroidal vorticity field ω_{0s}. The dashed line depicts the core boundary $r = 1$.

function of angles between the disturbance vorticity vector and the eigenvectors of the rate of strain for the first principal mode at $(k_0, \omega_0) \approx (0.8134868347, 0.5970895378)$. Tendency of alignment of the vorticity vector was recognized only with the unit toroidal vector. It follows that vortex-line stretching in the toroidal direction plays the leading role of driving instability.

The magnitude of strain increases with the distance r from the core center and takes its maximum at the core boundary $r = 1$. In the geometric-optics approximation, the growth rate for the wave-packet disturbance of short wavelength attains its maximum on the streamline circuiting the edge of the core (Hattori & Fukumoto 2003). In the short-wave limit, only the disturbance vorticity near the core boundary is relevant to the growth rate.

The growth rate of the principal modes diminishes as the branch label becomes larger. Calculation of intersection points of the dispersion curves and of the growth rate at the points is extended to large wavenumbers and is plotted in figure 4. The growth rate stays at relatively large values, approaching $\sigma_{1\max} \approx 0.02374715242$, along the two sequences of intersection points rapidly converging to $\omega_0 = 0.5$ (figure 4(a)). One sequence is intersection points between the i-th cograde mode of $m = 0$ and the i-th retrograde mode of $m = 1$ for which the growth rate monotonically decreases with k_0, and the other sequence is a collection of intersection points between the $(i+1)$-th cograde mode of $m = 0$ and the i-th retrograde mode of $m = 1$ for which the growth rate is, except for a first few intersection points, an increasing function of k_0. Eloy & Le Dizès (2001) called the latter the *principal modes*. We include both into the principal modes.

In order to grasp overall instability characteristics in the (k_0, ω_0) space, calculation of degenerate eigenvalues of the ith-ith radial modes of $(m, m+1)$ resonance is carried out

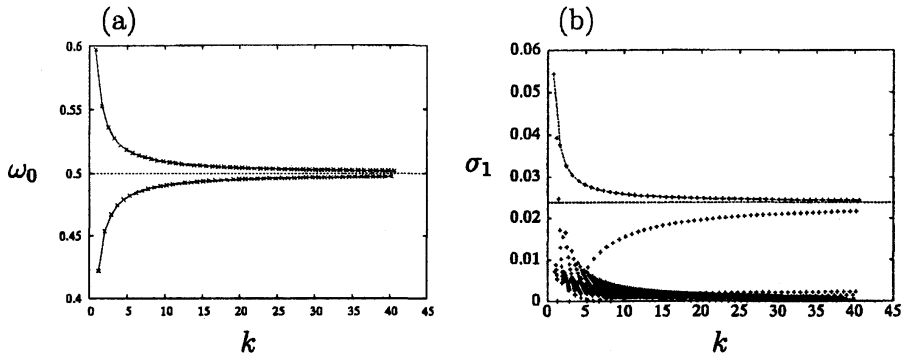

Figure 4: Large wavenumber behaviour of the (0, 1) resonance. (a) The intersection points (k_0, ω_0) of the dispersion curves, (b) The maximum growth rate $\sigma_{1\max}$.

over a wide range of k_0 and m. The growth rate is plotted in figure 5. The modes of $m = 1, 2, \cdots, 10$ and $20, 30, \cdots, 60$ are shown. Given m, the growth rate of $(m, m+1)$ resonance decreases with the branch label or the wavenumber k_0 and tends to $\sigma_{1\max} \approx 0.02374715242$ as $k_0 \to \infty$. On the other hand, given the branch label, the growth rate increases monotonically with m and approaches $\sigma_{1\max} = 0.64453125$ as $m \to \infty$. The ways of approach to the two different short-wave limits will be expounded in §5.

4.2 Energetics

Krein's theory of Hamiltonian spectra underlies the preceding numerical results. A necessary condition for loss of stability at a double eigenvalue is either that the eigenfunction consists of waves with opposite signed energy or that the eigenvalue is 0 (MacKay 1986; Dellnitz, Melbourne & Marsden 1992; Knobloch, Mahalov & Marsden 1994).

By taking advantage of Cairns' formula (Cairns 1979), Fukumoto (2003) reached a tidy expression for energy required to excite the Kelvin wave of azimuthal wavenumber m as

$$E = \frac{2\pi\omega_0}{\omega_0 - m}\left\{1 + \frac{(k_0/\eta_1)^2 K_{|m|}(k_0)}{k_0 K_{|m|-1}(k_0) + |m| K_{|m|}(k_0)}\left[\frac{2(\omega_0+m)}{\omega_0 - m} + \left(\frac{m(\omega_0+m)}{2} + k_0^2\right)\frac{K_{|m|}(k_0)}{k_0 K_{|m|-1}(k_0) + |m| K_{|m|}(k_0)}\right]\right\}\left(f_0^{(1)}\right)^2, \quad (4.1)$$

where $f_0^{(1)}$ is the displacement amplitude of the disturbed core $r = 1 + f_0^{(1)} \exp[i(m\theta + k_0 z - \omega_0 t)]$, and is linked to the amplitude $\beta_0^{(1)}$ of the disturbance pressure through

$$f_0^{(1)} = \frac{1}{4 - (\omega_0 - m)^2}\left\{-\eta_m J_{|m|-1}(\eta_m) + \frac{|m|}{\omega_0 - m}\left(\omega_0 - m + \frac{2m}{|m|}\right) J_{|m|}(\eta_m)\right\}\beta_0^{(1)}. \quad (4.2)$$

By a computation of the above formula, we find that the energy of the axisymmetric wave is all positive. At a given k_0, the i-th branch of negative mode ($\omega_0 < 0$) has the same

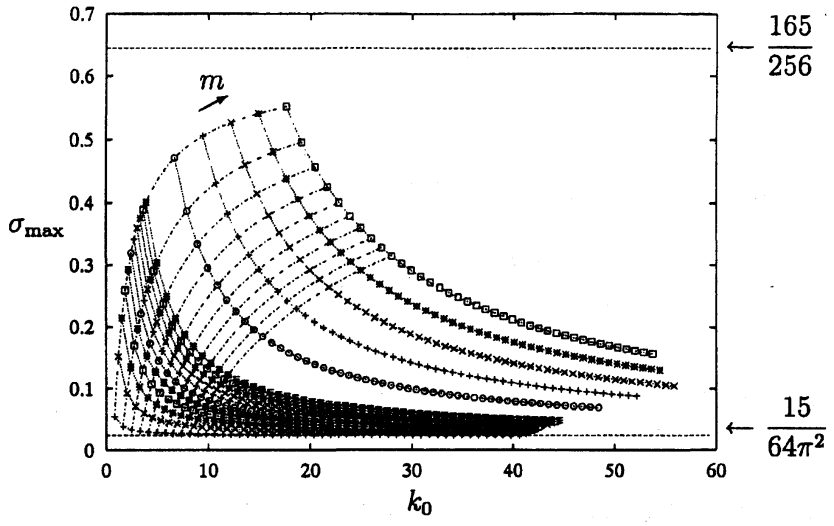

Figure 5: The growth rate of the principal modes between the i-th cograde modes of m wave and the i-th retrograde modes of $m+1$ wave. The same symbol is used for the same azimuthal wavenumber pair $(m, m+1)$. The lowest sequence (+) corresponds to $m = 0$. The highest sequence (□) corresponds to $m = 60$.

energy as the i-th branch of positive mode. The energy of the bending wave ($m = 1$) was illustrated in figure 8 of Fukumoto (2003). The energy of the isolated mode and cograde radial modes of $m = 1$ is positive over the entire range of k_0, and therefore resonance with the $m = 0$ mode is ruled out. As is evident from (4.1), alteration of energy sign occurs at the point, k_0^* say, where a dispersion curve crosses the k_0 axis. The energy of retrograde radial modes of $m = 1$ is negative in the range $0 < k_0 < k_0^*$, and is positive for $k_0 > k_0^*$. Eigenvalue collisions of negative- and positive-energy modes occur only between retrograde radial modes of $m = 1$ and upgoing modes of $m = 0$ in frequency range of $0 < \omega_0 < 1$, being in no contradiction with the numerical example of §4.1.

Krein's criterion by means of the energy signature furnishes merely a necessary condition for instability, yet it in effect serves as a sufficient condition for instability as well. The same is true of the MSTW instability (Fukumoto 2003).

5 Short-wavelength asymptotics

The expression (3.18) of growth rate suggests that a resonance pair with ω_0 closer to $m + 1/2$ is more influential. A universal feature manifests itself in the short wavelength limit in which ω_0 converges to $m + 1/2$. Here we omit the derivation. The detail is found in Fukumoto & Hattori (2004).

We have two wavelengths at our disposal, namely, the axial and the azimuthal wavelengths, and there are two ways of taking short wavelength limit. We begin with simple

azimuthal structure by fixing m, and thereafter we turn to the limit of $m \to \infty$.

5.1 Large k_0 with m fixed

Let l_1 and l_2 be large integers indexing branches of the m and the $m+1$ waves respectively as k_0 with m fixed. Define

$$\Delta l = l_2 - l_1\,, \quad \Delta' l = 2\Delta l - 1\,. \tag{5.1}$$

Asymptotic expansions of (k_0, ω_0) for degenerate eigenvalues of the $m, m+1$ waves are manipulated from the dispersion relation (A.7) and the counterpart of $m+1$. The intersection frequency is

$$\omega_0 = m + \frac{1}{2} + \frac{\sqrt{15}\pi\Delta' l}{128 k_0} - \frac{1}{128 k_0^2}\left\{m + \frac{1}{2} + \frac{\sqrt{15}\pi\Delta' l}{16}\right\} + O(k_0^{-3})\,. \tag{5.2}$$

The intersection wavenumber is obtained by solving iteratively

$$\begin{aligned} k_0 \;=\; & \frac{1}{\sqrt{15}}\left\{\frac{\pi(l_1 + l_2 + m - 1)}{2} + \arctan\left(\frac{1}{\sqrt{15}}\right)\right\} - \frac{1}{30 k_0}\left\{m^2 + m + 1 + \frac{29\pi^2(\Delta' l)^2}{256}\right\} \\ & + O(k_0^{-2})\,. \end{aligned} \tag{5.3}$$

Substituting from (5.2), (3.18) and (3.19) give,

$$\begin{aligned} \sigma_{1\max} \;=\; & \frac{15}{64\pi^2(\Delta' l)^2} + \frac{\sqrt{15}}{32 k_0}\left\{\frac{m}{\pi\Delta' l}\left[\frac{21}{8} + \frac{1}{\pi^2(\Delta' l)^2}\right] + \frac{1}{2}\left[-\frac{9\sqrt{15}}{64} + \frac{21}{8\pi\Delta' l}\right.\right. \\ & \left.\left. + \frac{\sqrt{15}}{16\pi^2(\Delta' l)^2} + \frac{1}{\pi^3(\Delta' l)^3}\right]\right\} + O(k_0^{-2})\,, \\ \Delta k_1 \;=\; & \frac{k_0}{2\pi^2(\Delta' l)^2} + \frac{m}{\sqrt{15}\pi\Delta' l}\left[\frac{21}{8} + \frac{1}{\pi^2(\Delta' l)^2}\right] + \frac{1}{2\sqrt{15}}\left[-\frac{9\sqrt{15}}{64} + \frac{21}{8\pi\Delta' l}\right. \\ & \left. + \frac{\sqrt{15}}{8\pi^2(\Delta' l)^2} + \frac{1}{\pi^3(\Delta' l)^3}\right] + O(k_0^{-1})\,. \end{aligned} \tag{5.4}$$

Finite value $15/(64\pi^2(\Delta' l)^2)$ of the growth rate is asymptoted in the limit of $k_0 \to \infty$, among which the modes specified by $\Delta l = 0$ and 1 have the largest growth rate $15/(64\pi^2) \approx 0.02374715242$. This limiting value is shared by all resonant pairs $(m, m+1)$ for finite values of m. These are the *principal modes* with slightly larger growth rate for $\Delta l = 1$. Correspondingly, the eigenfrequency ω_0 of the principal modes with $\Delta l = 0, 1$ achieves a relatively rapid convergence to the limit $\omega_0 = m + 1/2$ from below and above respectively as is seen from (5.2). The unstable wavenumber band, to leading order, broadens linearly in k_0, and this broad-band nature guarantees the validity of the geometric optics approach used by Hattori & Fukumoto (2003).

For the principal modes, (5.4) become, for $\Delta l = 1$,

$$\begin{aligned} \sigma_{1\max} \;&\approx\; 0.02374715242 + 0.02104135307/k_0\,, \\ \Delta k_1 \;&\approx\; 0.05066059182\, k_0 + 0.04805450688\,, \end{aligned} \tag{5.5}$$

and, for $\Delta l = 0$,

$$\begin{aligned} \sigma_{1\max} &\approx 0.02374715242 - 0.08399092777/k_0\,, \\ \Delta k_1 &\approx 0.05066059182\,k_0 - 0.1760143589\,, \end{aligned} \tag{5.6}$$

They fit fairly well with the values shown in figure 4.

Taking a careful look at figure 4(b) for the (0,1) resonance, modes other than the principal ones survive in the limit of $k_0 \to \infty$, which is confirmed from (5.4). This situation is contrasted with the MSTW instability for which the $\Delta l = 0$ mode holds a special status (Eloy & Le Dizès 2001; Fukumoto 2003).

Notice that the coefficients of correction terms in the asymptotic expansions (5.2), (5.3) and (5.4) grow with m, being indicative of nonuniformity in the expansions. At large values of m, a new regime shows up, in which vigorous modes reside.

5.2 Large k_0 and m with $\eta_1 \sim \eta_2 \sim m$

As $m \to \infty$, the intersection points (k_0, ω_0) between cograde radial modes of m and retrograde radial modes of $m+1$ are arranged so as to satisfy $\eta_1 \sim \eta_2 \sim m$ (Eloy & Le Dizès 2001). The asymptotic expansions for (k_0, ω_0) for those points are performed, to a high order in $1/m^{1/3}$, as

$$\begin{aligned} k_0 = {} & \frac{m}{\sqrt{15}} - \frac{a_1+a_2}{2^{4/3}\sqrt{15}}m^{1/3} + \frac{1}{56} + \frac{1}{2\sqrt{15}} - \frac{49(a_1^2+a_2^2) - 290a_1a_2}{640\cdot 2^{1/3}\sqrt{15}m^{1/3}} \\ & + \frac{1}{87808\cdot 2^{1/3}}\left[\frac{2}{3\sqrt{15}}(-64429a_1 + 42477a_2) - 725(a_1+a_2)\right]\frac{1}{m^{2/3}} + O(m^{-1})\,, \end{aligned} \tag{5.7}$$

$$\begin{aligned} \omega_0 = {} & m + \frac{1}{2} + \frac{15(a_1-a_2)}{64\cdot 2^{1/3}m^{2/3}} + \frac{435}{1792m} + \frac{3(a_1^2-a_2^2)}{64\cdot 2^{2/3}m^{4/3}} \\ & + \frac{5}{1404928\cdot 2^{1/3}}\left[2535\sqrt{15}(-a_1+a_2) + 169a_1 + 44073a_2\right]\frac{1}{m^{5/3}} + O(m^{-2})\,. \end{aligned} \tag{5.8}$$

In these, $a_1(<0)$ and $a_2(<0)$ are the zeros of the Airy function Ai and play the role of the branch labels for the m and the $m+1$ waves respectively. The first zero $a_1 \approx -2.338107410$ is tied with the first cograde radial mode of m and $a_2 \approx -2.338107410$ with the first retrograde radial mode of $m+1$.

A rapid approach to $\omega_0 = m + 1/2$ as $m \to \infty$ demands $\Delta a = a_2 - a_1 = 0$. They sit at the crossing points between the i-th branches of both m and $m+1$ radial waves, and thus are inherited from the principal modes of $\Delta l = 1$. The growth rate and the unstable band width for the case of $\Delta a = 0$ are, from (3.18) and (3.19),

$$\sigma_{1\max} = \frac{165}{256}\left(1 - \frac{33499\,|a_1|}{25872\times 2^{1/3}m^{2/3}}\right) + O\left(m^{-1}\right), \tag{5.9}$$

$$\Delta k_1 = \frac{11}{8\sqrt{15}}m\left(1 - \frac{7627\,|a_1|}{25872\times 2^{1/3}m^{2/3}}\right) + O\left(m^{0}\right). \tag{5.10}$$

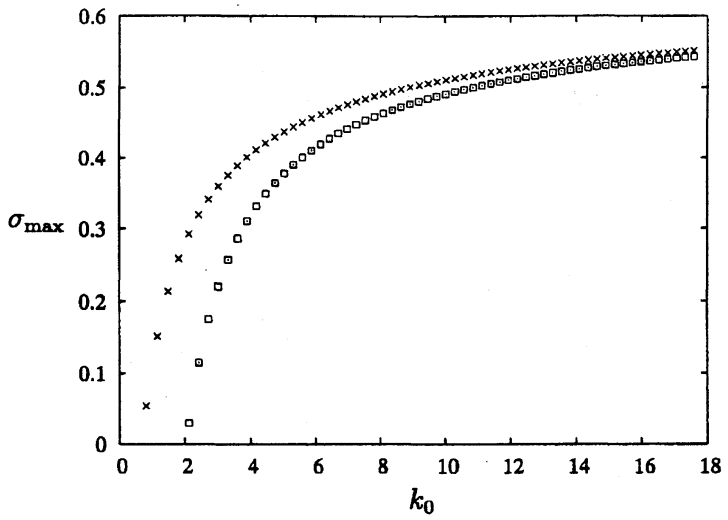

Figure 6: Variation of the maximum growth rate $\sigma_{1\max}$ with m for the resonance between the first-first radial modes of the m, $m+1$ waves. $m = 1, 2, \cdots, 60$. The short-wave asymptotics (5.11) and (5.7) are included with □.

The common value $\sigma_{1\max} = 165/256$ is asymptoted. Among them, the longest wave pair with $a_1 = a_2 \approx -2.338107410$, the first principal mode, has the largest growth rate

$$\sigma_{1\max} \approx 0.64453125 - 1.548698742/m^{2/3}, \tag{5.11}$$

$$\Delta k_1 \approx 0.3550234734\,m - 0.1942235728\,m^{1/3}. \tag{5.12}$$

This is the most dominant mode over the all possible resonance pairs. The way of increase, in m, of growth rate for the first principal mode is illustrated, with crosses, to $m = 60$ in figure 6. It is worth noting that $\sigma_{1\max} = 165/256$ was derived through the geometric optics approach by Hattori & Fukumoto (2003). The present solution supplies us with its structure globally in space.

In case $\Delta a = a_2 - a_1 \neq 0$, convergence of the eigenvalue to $\omega_0 = m + 1/2$ is slower. Modes with $\Delta a \neq 0$ vanish in the limit of $m \to \infty$.

A Kelvin waves

The expressions of the velocity field and the dispersion relation of Kelvin waves are collected in this appendix. The leading-order disturbance flow field of azimuthal wavenumber m is obtained in the form of normal mode as

$$\boldsymbol{v}_0 = \boldsymbol{v}_0^{(1)}(r)e^{im\theta}, \quad \pi_0 = \pi_0^{(1)}(r)e^{im\theta}, \quad \phi_0 = \phi_0^{(1)}(r)e^{im\theta}. \tag{A.1}$$

By integrating the linearized Euler equations outside and inside the core with radius given by (2.9), separately, we find that

$$\phi_0^{(1)} = K_m(k_0 r)\alpha_0^{(1)} \qquad \text{for } r > 1 + \tilde{f}_0\,, \tag{A.2}$$

and

$$\begin{aligned}
\pi_0^{(1)} &= J_m(\eta_1 r)\beta_0^{(1)}\,,\\
u_0^{(1)} &= \frac{i}{\omega_0 - m + 2}\left\{-\frac{m}{r}J_m(\eta_1 r) + \frac{\omega_0 - m}{\omega_0 - m - 2}\eta_1 J_{m+1}(\eta_1 r)\right\}\beta_0^{(1)}\,,\\
v_0^{(1)} &= \frac{1}{\omega_0 - m + 2}\left\{\frac{m}{r}J_m(\eta_1 r) + \frac{2}{\omega_0 - m - 2}\eta_1 J_{m+1}(\eta_1 r)\right\}\beta_0^{(1)}\,,\\
w_0^{(1)} &= \frac{k_0}{\omega_0 - m}J_m(\eta_1 r)\beta_0^{(1)} \qquad \text{for } r < 1 + \tilde{f}_0\,,
\end{aligned} \tag{A.3}$$

where the radial wavenumber η_1 is given by

$$\eta_1^2 = \left[4/(\omega_0 - m)^2 - 1\right]k_0^2\,, \tag{A.4}$$

and J_m and K_m are respectively the Bessel function of the first kind and the modified Bessel function of the second kind, m being their order, and $\alpha_0^{(1)}$ and $\beta_0^{(1)}$ are arbitrary constants. The non-singular conditions $\omega_0 \neq m$ and $\omega_0 \neq m \pm 2$ are to be kept in view. The radial wavenumber of the $m+1$ wave is

$$\eta_2^2 = \left[4/(\omega_0 - m - 1)^2 - 1\right]k_0^2\,. \tag{A.5}$$

The boundary conditions supply the relation between $\alpha_0^{(1)}$ and $\beta_0^{(1)}$ as

$$\alpha_0^{(1)} = -\frac{iJ_m(\eta_1)}{(\omega_0 - m)K_m(k_0)}\beta_0^{(1)}\,, \tag{A.6}$$

and the dispersion relation

$$J_{m+1}(\eta_1) = \left\{\frac{2m}{\omega_0 - m + 2} - \frac{k_0 K_{m+1}(k_0)}{K_m(k_0)}\right\}\frac{\eta_1}{k_0^2}J_m(\eta_1)\,. \tag{A.7}$$

B Closed-form solution for disturbance field and the solvability conditions

This appendix is concerned with the closed-form solution of the $O(\epsilon)$ disturbance field, the boundary conditions, and the solvability conditions for a possible parametric resonance between Kelvin waves with azimuthal wavenumbers m and $m+1$. The superscript 1 refers to the m wave, and 2 refers to the $m+1$ wave.

By inspection and with the help of computer algebra, a general solution of (3.13) for the m wave, finite at $r = 0$, is manipulated as

$$\begin{aligned}\pi_1^{(1)} &= J_m(\eta_1 r)\beta_1^{(1)} + \left\{\frac{4k_0^2\omega_1}{(\omega_0-m)^3} - \frac{\eta_1^2 k_1}{k_0}\right\}\frac{r}{\eta_1}J_{m+1}(\eta_1 r)\beta_0^{(1)} \\ &+\frac{i}{16}\left\{\left[5(r^2-1) + \frac{(\omega_0-m-1)^2(\omega_0-m)^2(\omega_0-m+2)}{2k_0^2(2\omega_0-2m-1)^2(\omega_0-m+1)}A_1\right]\eta_2 J_m(\eta_2 r)\right. \\ &\left.+\frac{A_2}{2\omega_0-2m-1}rJ_{m+1}(\eta_2 r)\right\}\beta_0^{(2)}, \end{aligned} \tag{B.1}$$

where $\beta_1^{(1)}$ is a constant and

$$\begin{aligned} A_1 &= 9\omega_0^4 - 18(2m+1)\omega_0^3 + (54m^2+54m+1)\omega_0^2 - 2(2m+1)(3m-2)(3m+5)\omega_0 \\ &\quad +9m^4+18m^3-23m^2-32m-8, \\ A_2 &= 9\omega_0^4 - 9(4m+1)\omega_0^3 + (54m^2+27m-26)\omega_0^2 - (36m^3+27m^2-56m-20)\omega_0 \\ &\quad +9m^4+9m^3-30m^2-22m-2. \end{aligned} \tag{B.2}$$

Returning to the Euler equations (3.1) and (3.2), the disturbance radial velocity $u_1^{(m)}$ is found to be

$$\begin{aligned} u_1^{(1)} &= i\left\{-\frac{mJ_m(\eta_1 r)}{(\omega_0-m+2)r} + \frac{1}{2}\left(\frac{1}{\omega_0-m+2}+\frac{1}{\omega_0-m-2}\right)\eta_1 J_{m+1}(\eta_1 r)\right\}\beta_1^{(1)} \\ &+\frac{i\omega_1}{(\omega_0-m+2)^2}\left\{\left[\frac{m}{r}+\frac{4\eta_1^2 r}{(\omega_0-m-2)^2}\right]J_m(\eta_1 r)\right. \\ &\quad\left.-\frac{1}{(\omega_0-m-2)^2}\left[\omega_0^2-2m\omega_0+(m+2)^2+\frac{8m}{\omega_0-m}\right]\eta_1 J_{m+1}(\eta_1 r)\right\}\beta_0^{(1)} \\ &-ik_1\left\{\frac{k_0}{\omega_0-m}rJ_m(\eta_1 r)+\frac{m}{k_0(\omega_0-m-2)}\eta_1 J_{m+1}(\eta_1 r)\right\}\beta_0^{(1)} \\ &+\frac{1}{16}\left\{\frac{1}{\omega_0-m+1}\left[m\left(\frac{(\omega_0-m)^2(\omega_0-m-1)^2}{2k_0^2(2\omega_0-2m-1)^2}A_1-5\right)\frac{1}{r}\right.\right. \\ &\quad\left.+\frac{A_3}{(\omega_0-m-3)(2\omega_0-2m-1)}r\right]\eta_2 J_m(\eta_2 r) \\ &\quad\left.+\left[\frac{A_4}{2(\omega_0-m-3)(2\omega_0-2m-1)^2}+\frac{5k_0^2}{\omega_0-m-1}(r^2-1)\right]J_{m+1}(\eta_2 r)\right\}\beta_0^{(2)}, \end{aligned} \tag{B.3}$$

where

$$\begin{aligned} A_3 &= 9\omega_0^5 - 9(5m+3)\omega_0^4 + (90m^2+108m+1)\omega_0^3 - (90m^3+162m^2-11m-11)\omega_0^2 \\ &\quad +(45m^4+108m^3-25m^2-63m+14)\omega_0 - 9m^5-27m^4+13m^3+52m^2+3m-8, \\ A_4 &= 9\omega_0^8 - 18(4m+3)\omega_0^7 + 2(126m^2+189m+41)\omega_0^6 - 2(252m^3+567m^2+252m \end{aligned}$$

$$
\begin{aligned}
&-8)\omega_0^5 + (630m^4 + 1890m^3 + 1290m^2 - 98m - 87)\omega_0^4 \\
&-2(252m^5 + 945m^4 + 880m^3 - 116m^2 - 262m - 27)\omega_0^3 \\
&+2(126m^6 + 567m^5 + 675m^4 - 134m^3 - 533m^2 - 154m + 18)\omega_0^2 \\
&-2(36m^7 + 189m^6 + 276m^5 - 76m^4 - 454m^3 - 235m^2 + 32m + 28)\omega_0 \\
&+9m^8 + 54m^7 + 94m^6 - 34m^5 - 279m^4 - 216m^3 + 24m^2 + 68m + 16\,. \qquad \text{(B.4)}
\end{aligned}
$$

Substituting from (3.11), (B.1), (B.3) and the expressions in Appendix A and evaluating them at $r = 1$, the boundary conditions (3.16) for the m wave are converted into linear algebraic equations for $\alpha_1^{(1)}$ and $\beta_1^{(1)}$:

$$
\begin{bmatrix} mK_m - k_0K_{m+1} & \frac{i}{\omega_0-m+2}\left[mJ_m(\eta_1) - \frac{\omega_0-m}{\omega_0-m-2}\eta_1 J_{m+1}(\eta_1)\right] \\ -i(\omega_0-m)K_m & J_m(\eta_1) \end{bmatrix} \begin{bmatrix} \alpha_1^{(1)} \\ \beta_1^{(1)} \end{bmatrix} = \begin{bmatrix} F^{(1)} \\ G^{(1)} \end{bmatrix}, \qquad \text{(B.5)}
$$

where we have made use of the shorthand notation $K_m = K_m(k_0)$ and $K_{m+1} = K_{m+1}(k_0)$. The dispersion relation (A.7) helps to simplify $F^{(1)}$ and $G^{(1)}$ by eliminating $J_{m+1}(\eta_1)$ from these equations.

As is usually the case, the matrix in (B.5) is singular, and hence the vector $(F^{(1)}, G^{(1)})$ must be constrained to its image space in order for (B.5) to be solvable for $(\alpha_1^{(1)}, \beta_1^{(1)})$. This solvability condition reads

$$
i(\omega_0 - m)F^{(1)} + \left(m - \frac{k_0K_{m+1}}{K_m}\right) G^{(1)} = 0\,. \qquad \text{(B.6)}
$$

The same procedure is repeated for the $m+1$ wave.

These conditions are rewritten into homogeneous linear algebraic equations for $\beta_0^{(1)}$ and $\beta_0^{(2)}$ as

$$
\begin{aligned}
&\left\{\frac{\omega_1 f^{(1)}}{(\omega_0-m+2)(\omega_0-m-2)} + \frac{2k_1}{k_0}(\omega_0-m)g^{(1)}\right\}\beta_0^{(1)} \\
&\qquad + \frac{i(\omega_0-m)^4 J_{m+1}(\eta_2)}{32k_0^2(2\omega_0-2m-1)^2(\omega_0-m-1)J_m(\eta_1)} h\beta_0^{(2)} = 0\,, \qquad \text{(B.7)} \\
&-\frac{i(\omega_0-m-1)^4 J_m(\eta_1)}{32k_0^2(2\omega_0-2m-1)^2(\omega_0-m)J_{m+1}(\eta_2)} h\beta_0^{(1)} \\
&\qquad + \left\{\frac{\omega_1 f^{(2)}}{(\omega_0-m+1)(\omega_0-m-3)} + \frac{2k_1}{k_0}(\omega_0-m-1)g^{(2)}\right\}\beta_0^{(2)} = 0\,. \qquad \text{(B.8)}
\end{aligned}
$$

In these,

$$
\begin{aligned}
f^{(1)} \;=\; & m[\omega_0^3 - (3m+4)\omega_0^2 + 3m^2\omega_0 - m(m^2-4m-8)] + 2k_0^2(\omega_0-m)^2 \\
& +4[(m+1)\omega_0^2 - 2m^2\omega_0 + m(m^2-m-4)]\frac{k_0K_{m+1}}{K_m} \\
& -2(\omega_0-m+2)(\omega_0-m-2)\frac{k_0^2K_{m+1}^2}{K_m^2}\,, \qquad \text{(B.9)}
\end{aligned}
$$

$$f^{(2)} = (m+1)[\omega_0^3 - (3m-1)\omega_0^2 + 3(m+1)^2\omega_0 - m^3 - 7m^2 - 3m + 3]$$
$$+2k_0^2(\omega_0 - m - 1)^2 - 4[m\omega_0^2 - 2(m+1)^2\omega_0 + (m+1)(m^2+3m-2)]\frac{k_0K_m}{K_{m+1}}$$
$$-2(\omega_0 - m + 1)(\omega_0 - m - 3)\frac{k_0^2K_m^2}{K_{m+1}^2}, \qquad \text{(B.10)}$$

$$g^{(1)} = -\left(m - \frac{k_0K_{m+1}}{K_m}\right)\left[m(\omega_0 - m - 1) + \frac{k_0K_{m+1}}{K_m}\right], \qquad \text{(B.11)}$$

$$g^{(2)} = \left(m + 1 + \frac{k_0K_m}{K_{m+1}}\right)\left[(m+1)(\omega_0 - m) + \frac{k_0K_m}{K_{m+1}}\right], \qquad \text{(B.12)}$$

$$h = (\omega_0 - m)(\omega_0 - m - 1)\Big\{(m+1)(\omega_0 - m + 2)\frac{k_0K_{m+1}}{K_m} + m(\omega_0 - m - 3)\frac{k_0K_m}{K_{m+1}}$$
$$-2m(m+1)\Big\}A_1 + 2k_0^2A_5 + (2\omega_0 - 2m - 1)k_0^3\Big\{[A_1 - 6(3\omega_0^2 - 3\omega_0 - 3m^2 + 1)]\frac{K_{m+1}}{K_m}$$
$$-[A_1 - 6(3\omega_0^2 + 3\omega_0 - 3m^2 - 6m - 2)]\frac{K_m}{K_{m+1}}\Big\}, \qquad \text{(B.13)}$$

where

$$A_5 = 9\omega_0^6 - 36(2m+1)\omega_0^5 + (225m^2 + 225m + 46)\omega_0^4 - 9(2m+1)(20m^2 + 20m - 3)\omega_0^3$$
$$+(315m^4 + 630m^3 + 126m^2 - 189m - 38)\omega_0^2$$
$$-m(m+1)(2m+1)(72m^2 + 72m - 115)\omega_0$$
$$+27m^6 + 81m^5 + 12m^4 - 111m^3 - 71m^2 - 2m + 4. \qquad \text{(B.14)}$$

References

[1] BAYLY, B. J. 1986 Three-dimensional instability of elliptical flow. *Phys. Rev. Lett.* **57**, 2160–2163.

[2] CAIRNS, R. A. 1979 The role of negative energy waves in some instabilities of parallel flows. *J. Fluid Mech.* **92**, 1–14.

[3] DELLNITZ, M., MELBOURNE, I. & MARSDEN, J. E. 1992 Generic bifurcation of Hamiltonian vector fields with symmetry. *Nonlinearity* **5**, 979–996.

[4] ELOY, C. & LE DIZÈS, S. 2001 Stability of the Rankine vortex in a multipolar strain field. *Phys. Fluids* **13**, 660–676.

[5] FUKUMOTO, Y. 2002 Higher-order asymptotic theory for the velocity field induced by an inviscid vortex ring. *Fluid Dyn. Res.* **30**, 67–95.

[6] FUKUMOTO, Y. 2003 The three-dimensional instability of a strained vortex tube revisited. *J. Fluid Mech.* **493**, 287–318.

[7] FUKUMOTO, Y. & HATTORI, Y. 2002 Linear stability of a vortex ring revisited. In *Proc. of IUTAM Symposium on Tubes, Sheets and Singularities in Fluid Dynamics* (eds. H. K. Moffatt and K. Bajer), pp. 37–48. Kluwer.

[8] FUKUMOTO, Y. & HATTORI, Y. 2004 Curvature instability of a vortex ring. *preprint.*

[9] FUKUMOTO, Y. & MOFFATT, H. K. 2000 Motion and expansion of a viscous vortex ring. Part 1. A higher-order asymptotic formula for the velocity. *J. Fluid Mech.* **417**, 1–45.

[10] HATTORI, Y. & FUKUMOTO, Y. 2003 Short-wavelength stability analysis of thin vortex rings. *Phys. Fluids.* **15**, 3151–3163.

[11] KNOBLOCH, E., MAHALOV, A. & MARSDEN, J. E. 1994 Normal forms for three-dimensional parametric instabilities in ideal hydrodynamics. *Physica D* **73**, 49–81.

[12] MACKAY, R. S. 1986 Stability of equilibria of Hamiltonian systems. In *Nonlinear Phenomena and Chaos* (ed. S. Sarkar), pp. 254–270. Adam Hilger, Bristol.

[13] MOORE, D. W. & SAFFMAN, P. G. 1975 The instability of a straight vortex filament in a strain field. *Proc. R. Soc. Lond. A* **346**, 413–425.

[14] SAFFMAN, P. G. 1992 *Vortex Dynamics*, Chap. 12. Cambridge University Press.

[15] TSAI, C.-Y. & WIDNALL, S. E. 1976 The stability of short waves on a straight vortex filament in a weak externally imposed strain field. *J. Fluid Mech.* **73**, 721–733.

[16] WALEFFE, F. 1990 On the three-dimensional instability of strained vortices. *Phys. Fluids A* **2**, 76-80.

[17] WIDNALL, S. E., BLISS, D. B. & TSAI, C.-Y. 1974 The instability of short waves on a vortex ring. *J. Fluid Mech.* **66**, 35–47.

[18] WIDNALL, S. E. & TSAI, C.-Y. 1977 The instability of the thin vortex ring of constant vorticity. *Phil. Trans. R. Soc. Lond. A* **287**, 273–305.